Regularized Least-Squares SPECT Image Reconstruction Using Multiresolution Spatial B-Splines and a Negativity Penalty

Bryan W. Reutter, Grant T. Gullberg, Rostyslav Boutchko, Karthikayan Balakrishnan, Elias H. Botvinick, and Ronald H. Huesman

***Abstract*—We investigated the benefit of incorporating a negativity penalty into a least-squares criterion used to reconstruct 3-D radiotracer distributions in cardiac SPECT studies. B-spline spatial basis functions were used to provide a continuous model for the 3-D tracer distribution. Spline coefficients that tended to have negative values were identified and were constrained to stay near zero with use of a quadratic penalty that penalized nonzero contributions to the projection data model. To test the method we used trilinear B-splines to reconstruct volumetric images for a ^{99m}Tc-sestamibi cardiac SPECT/CT patient study. Spline coefficients were estimated by minimizing a least-squares criterion by direct matrix inversion via Cholesky decomposition. Volumetric images were reconstructed both with and without the negativity penalty, using (1) a higher-resolution spline basis and (2) a multiresolution basis composed of higher-resolution splines in the heart volume and lower-resolution splines elsewhere. Reduced image noise and good myocardial resolution were obtained with use of the multiresolution basis. Use of the penalty dramatically reduced image noise for the higher-resolution basis and yielded good resolution throughout the body. Encouraged by these results, we are using multiresolution 4-D spatiotemporal B-splines and penalized weighted least-squares inversion to reconstruct dynamic SPECT data from rest/stress cardiac patient studies.**

***Index Terms*—Penalized least-squares, SPECT/CT, fully three-dimensional reconstruction, B-spline basis functions.**

I. Introduction

We investigated the benefit of incorporating a negativity penalty into a least-squares criterion used to reconstruct 3-D radiotracer distributions in cardiac single-photon emission computed tomography (SPECT) studies. B-spline spatial basis functions were used to provide a continuous model for the 3-D tracer distribution [1]. Spline coefficients that tended to have negative values were identified with use of an iterative algorithm that converged quickly. These coefficients were then constrained to stay near zero with use of a quadratic penalty that penalized nonzero contributions to the projection data model.

This work was supported by the National Institutes of Health under grants R01-HL50663 and R01-HL71253 and by the Director, Office of Science, Office of Biological and Environmental Research, Medical Sciences Division of the U. S. Department of Energy under contract DE-AC03-76SF00098.

B. W. Reutter, G. T. Gullberg, R. Boutchko, K. Balakrishnan, and R. H. Huesman are with the Department of Medical Imaging Technology, Lawrence Berkeley National Laboratory, Berkeley, CA 94720 USA (e-mail: BWReutter@lbl.gov, GTGullberg@lbl.gov, RBuchko@lbl.gov, KBalakrishnan@lbl.gov, RHHuesman@lbl.gov).

E. H. Botvinick is with the Departments of Radiology and Medicine, University of California, San Francisco, CA 94143 USA.

This approach is motivated by goals of achieving a well-posed image reconstruction problem and computational efficiency. To test the method we used trilinear B-splines to reconstruct volumetric images for a ^{99m}Tc-sestamibi cardiac SPECT/CT patient study. Attenuation and depth-dependent point response were modeled. Volumetric images were reconstructed both with and without the negativity penalty, using (1) a higher-resolution basis composed of more-spatially-compact splines and (2) a multiresolution basis composed of more-spatially-compact splines in the heart volume and less-spatially-compact splines elsewhere. Reduced image noise and good myocardial resolution were obtained with use of the multiresolution basis. Use of the penalty dramatically reduced image noise for the higher-resolution basis and yielded good resolution throughout the body.

II. Regularized Least-Squares Reconstruction with Negativity Penalty

A SPECT projection data model that relates detected events to a spatial B-spline representation of the 3-D radiotracer distribution can be written as

$$\mathbf{p} = \mathbf{F}\mathbf{a}, \tag{1}$$

where $\mathbf{p}$ is an I-element column vector of modeled projection values, $\mathbf{F}$ is an $I \times M$ system matrix, $\mathbf{a}$ is an M-element column vector of spline coefficients, I is the total number of projection measurements acquired by the SPECT detector(s), and M is the number of spline basis functions spanning the image volume to be reconstructed. The system matrix $\mathbf{F}$ incorporates physical effects such as attenuation, depth-dependent collimator response, and scatter that affect detection of gamma rays emitted by the radiotracer distribution.

At the outset, the least-squares criterion to be minimized, χ^2, is simply the sum of squared differences between the measured projections, $\mathbf{p}^*$, and the modeled projections:

$$\chi^2 = (\mathbf{p}^* - \mathbf{F}\mathbf{a})^{\mathrm{T}}(\mathbf{p}^* - \mathbf{F}\mathbf{a}), \tag{2}$$

where the superscript "T" denotes the matrix transpose. Minimizing the criterion χ^2 yields an estimate, $\hat{\mathbf{a}}$, of coefficients for the spline basis functions that represent the 3-D radiotracer distribution:

$$\hat{\mathbf{a}} = (\mathbf{F}^{\mathrm{T}}\mathbf{F})^{-1}\mathbf{F}^{\mathrm{T}}\mathbf{p}^*. \tag{3}$$

The corresponding minimum value for the criterion χ^2 is

$$\chi^2_{\min} = (\mathbf{p}^* - \mathbf{F}\hat{\mathbf{a}})^{\mathrm{T}}(\mathbf{p}^* - \mathbf{F}\hat{\mathbf{a}}). \tag{4}$$

Generally speaking, some of the coefficients in the estimate $\hat{\mathbf{a}}$ may have relatively large negative values, particularly for very noisy projection data measurements $\mathbf{p}^*$. To constrain these non-physiological values we wish to add a term to the criterion χ^2 that penalizes negative values. Insight into what a reasonable penalty term might be can be obtained by expressing χ^2 in terms of its minimum value:

$$\begin{aligned}\chi^2 &= (\mathbf{p}^* - \mathbf{F}\mathbf{a})^{\mathrm{T}}(\mathbf{p}^* - \mathbf{F}\mathbf{a}) \\ &= [(\mathbf{p}^* - \mathbf{F}\hat{\mathbf{a}}) - \mathbf{F}(\mathbf{a} - \hat{\mathbf{a}})]^{\mathrm{T}}[(\mathbf{p}^* - \mathbf{F}\hat{\mathbf{a}}) - \mathbf{F}(\mathbf{a} - \hat{\mathbf{a}})] \\ &= \chi^2_{\min} - 2(\mathbf{p}^* - \mathbf{F}\hat{\mathbf{a}})^{\mathrm{T}}\mathbf{F}(\mathbf{a} - \hat{\mathbf{a}}) + (\mathbf{a} - \hat{\mathbf{a}})^{\mathrm{T}}\mathbf{F}^{\mathrm{T}}\mathbf{F}(\mathbf{a} - \hat{\mathbf{a}}) \\ &= \chi^2_{\min} + (\mathbf{a} - \hat{\mathbf{a}})^{\mathrm{T}}\mathbf{F}^{\mathrm{T}}\mathbf{F}(\mathbf{a} - \hat{\mathbf{a}}).\end{aligned} \tag{5}$$

Note that the term in eqn. (5) that is linear with respect to $(\mathbf{a} - \hat{\mathbf{a}})$ vanishes (i.e., the model error $\mathbf{p}^* - \mathbf{F}\hat{\mathbf{a}}$ lies in the null space of the backprojection operator $\mathbf{F}^{\mathrm{T}}$).

Examining eqn. (5), one sees that deviation of $\mathbf{a}$ away from $\hat{\mathbf{a}}$ increases χ^2 by an amount $(\mathbf{a} - \hat{\mathbf{a}})^{\mathrm{T}}\mathbf{F}^{\mathrm{T}}\mathbf{F}(\mathbf{a} - \hat{\mathbf{a}})$. To mimic this effect for purposes of constraining negative values, we now define the criterion, ψ^2, which adds a term to χ^2 that penalizes deviations of certain elements of $\mathbf{a}$ away from zero:

$$\psi^2 = \chi^2 + \mathbf{a}^{\mathrm{T}}\mathbf{N}\mathbf{F}^{\mathrm{T}}\mathbf{F}\mathbf{N}\mathbf{a}, \tag{6}$$

where the $M \times M$ matrix $\mathbf{N}$ is a diagonal matrix whose (m, m)-th element is one if the penalty is to be applied to the m-th element of $\mathbf{a}$, or is zero if the penalty is not to be applied to the m-th element of $\mathbf{a}$. In essence, the additional term penalizes nonzero contributions to the projection data model resulting from the forward projection, $\mathbf{F}\mathbf{N}\mathbf{a}$, of spatial spline basis functions whose coefficients are flagged by the diagonal elements of $\mathbf{N}$.

Thus, if the matrix $\mathbf{N}$ is properly defined the criterion ψ^2 tends to drive coefficients of $\hat{\mathbf{a}}$, which would be negative without the penalty, closer to zero. Note that there is no arbitrary multiplicative scaling factor (i.e., hyperparameter) applied to the penalty term, as the term appears to be already properly scaled with respect to χ^2 by virtue of eqn. (5).

Given the matrix $\mathbf{N}$, the criterion ψ^2 is minimized by

$$\tilde{\mathbf{a}} = (\mathbf{F}^{\mathrm{T}}\mathbf{F} + \mathbf{N}\mathbf{F}^{\mathrm{T}}\mathbf{F}\mathbf{N})^{-1}\mathbf{F}^{\mathrm{T}}\mathbf{p}^*. \tag{7}$$

The matrix $\mathbf{N}$ can be defined and a penalized least-squares estimate $\tilde{\mathbf{a}}$ can be obtained in a few iterations as follows:

1) Initialize $\mathbf{N}$ to be a zero matrix.
2) Minimize the criterion χ^2 in eqn. (2) via direct matrix inversion [eqn. (3)] to obtain the estimate $\hat{\mathbf{a}}$.
3) Set diagonal elements of $\mathbf{N}$ corresponding to negative elements of $\hat{\mathbf{a}}$ to one.
4) Minimize the criterion ψ^2 in eqn. (6) via direct matrix inversion [eqn. (7)] to obtain an estimate $\tilde{\mathbf{a}}$.
5) Set diagonal elements of $\mathbf{N}$ corresponding to negative elements of $\tilde{\mathbf{a}}$ to one, if they are not already one. Once a diagonal element of $\mathbf{N}$ has been set to one, it should remain at one even if the corresponding element in $\tilde{\mathbf{a}}$ swings positive.
6) Repeat steps 4 and 5 until the matrix $\mathbf{N}$ does not change. The resulting estimate $\tilde{\mathbf{a}}$ is the "final" estimate.

For the $^{99\mathrm{m}}$Tc-sestamibi cardiac SPECT/CT patient study described in Section IV, the matrix $\mathbf{N}$ converged in 4–7 iterations of steps 4 and 5. Inversion of the symmetric, positive definite matrices in eqns. (3) and (7) can be accomplished relatively quickly and robustly with use of Cholesky decomposition [2].

III. Properties of Uniform B-Splines

Use of splines and other "blob"-like basis functions in tomographic image reconstruction has been an active area of research (e.g., [3]–[5]), as has been use of multiresolution reconstruction grids (e.g., [6]).

The kth-order uniform B-spline basis function, $\Pi^{*k}(x)$, is the piecewise $(k-1)$st-degree polynomial that is obtained by convolving the rectangle function

$$\Pi(x) = \begin{cases} 1 & x \in \left[-\frac{1}{2}, \frac{1}{2}\right) \\ 0 & \text{otherwise} \end{cases} \tag{8}$$

with itself $k-1$ times (Fig. 1) [7], [8]. The Gaussian is obtained in the limit as the order k approaches infinity. The function $\Pi^{*k}(x)$ has a support of width k, a standard deviation of $\sqrt{k/12}$, and unit integral (i.e., $\int_{-\infty}^{\infty} \Pi^{*k}(x)dx = 1$). The appropriately scaled function having a support of width ak, a standard deviation of $a\sqrt{k/12}$, and unit integral is $\frac{1}{a}\Pi^{*k}\left(\frac{x}{a}\right)$, for $a > 0$. The Fourier transform of $\frac{1}{a}\Pi^{*k}\left(\frac{x}{a}\right)$ is $\mathrm{sinc}^k(as)$.

The support of the kth-order uniform B-spline basis function $\frac{1}{a}\Pi^{*k}\left(\frac{x}{a}\right)$ can be doubled simply by taking a linear combination of $k+1$ shifted versions of itself:

$$\frac{1}{2a}\Pi^{*k}\left(\frac{x}{2a}\right) = \frac{1}{2^k}\sum_{j=0}^{k}\binom{k}{j}\left[\frac{1}{a}\Pi^{*k}\left(\frac{x}{a} + \frac{k}{2} - j\right)\right]. \tag{9}$$

Thus, in tomographic imaging the forward-projection matrix for lower-resolution splines is just a linear combination of the columns of a matrix for higher-resolution splines [1].

IV. $^{99\mathrm{m}}$Tc-Sestamibi Cardiac SPECT/CT Patient Study

For computational simplicity, we used separable, trilinear B-spline spatial basis functions [i.e., products of the form $\Pi^{*2}(x)\Pi^{*2}(y)\Pi^{*2}(z)$] to reconstruct volumetric images for a $^{99\mathrm{m}}$Tc-sestamibi cardiac SPECT/CT patient study. Because the B-splines overlap one another in all three spatial dimensions, a fully 3-D reconstruction must be performed.

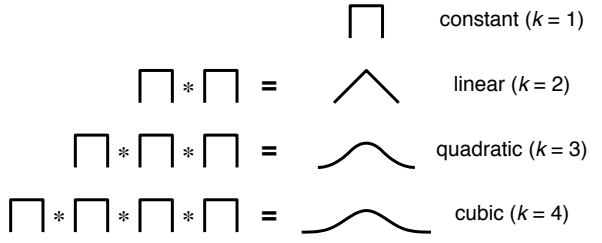

Fig. 1. The kth-order uniform B-spline is obtained by convolving the rectangle function with itself $k-1$ times.

A. SPECT/CT Data Acquisition

Emission data were acquired with use of parallel-hole collimators on a dual-head GE Millennium VH Hawkeye SPECT/CT scanner. A 30 min dynamic scan was performed, with the patient's arms down for comfort, subsequent to pharmacologically induced stress as part of a rest/stress protocol. During the scan, the gantry performed 24 360-degree rotations, acquiring 72 views per rotation at 1 sec per view. Projections at each view were binned into frames of 64×64 pixels, with pixel size 8.84 mm × 8.84 mm. For this investigation, data acquired 2.4–30 min post-injection (i.e., during the last 22 rotations) were summed to obtain a static dataset. Volumetric images were reconstructed from projections of the heart obtained in 64 (transverse) × 9 (axial) sub-frames of the 72 views, which contained a total of about 6.8 million detected events (Fig. 2). An X-ray CT scan was performed with use of the integrated Hawkeye system to obtain an attenuation map (Fig. 3).

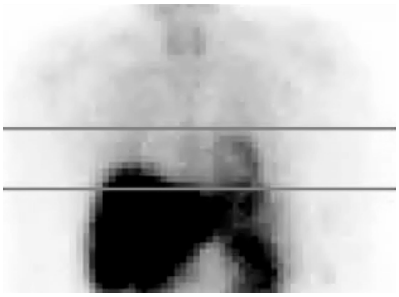

Fig. 2. Anterior view of summed late projection data from a ^{99m}Tc-sestamibi cardiac SPECT patient study. Gray lines depict the 8 cm axial extent of the volume in which the radiotracer distribution was estimated via fully 3-D reconstruction.

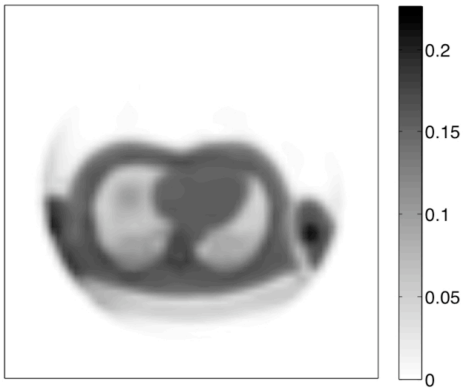

Fig. 3. Smoothed attenuation map for a transverse mid-ventricular slice acquired by the integrated Hawkeye X-ray CT system.

B. B-Spline Image Space Models

A higher-resolution model for image space composed of more-spatially-compact B-splines was obtained by first thresholding the attenuation map to obtain a mask for the patient's body and the bed. The volume encompassed by the mask was then spanned by 7659 overlapping trilinear B-splines organized on a 63×63×5 rectangular grid having a spacing of 8.84 mm × 8.84 mm × 17.7 mm along the x-, y-, and z-axes, respectively, where x and y are transverse coordinates and z is the axial coordinate. The overlapping splines had a support of 17.7 mm × 17.7 mm × 35.4 mm along x, y, and z, respectively.

A multiresolution spatial model was obtained by first doubling the transverse support of the higher-resolution splines via eqn. (9) and downsampling in the transverse plane. This yielded a total of 2201 overlapping trilinear B-splines organized on a 31×31×5 rectangular grid having a spacing of 17.7 mm × 17.7 mm × 17.7 mm along x, y, and z, respectively. The overlapping splines had a support of 35.4 mm × 35.4 mm × 35.4 mm along x, y, and z, respectively. A 6×6×5 neighborhood of lower-resolution splines that spanned the heart volume was then replaced with an 11×11×5 neighborhood of higher-resolution splines, to obtain a total of 2626 spatial basis functions.

C. Projection Data Models, Penalized Least-Squares Minimization, and Reconstructed Images

For the higher-resolution spatial basis, a system model that related spatial spline intensities to detected events was calculated with use of a fully 3-D ray-driven projector [9] that modeled depth-dependent collimator response, as well as attenuation based on the measured attenuation map. Scatter was not modeled. This resulted in a projection data model $\mathbf{Fa} = \mathbf{p}$, where $\mathbf{F}$ is a 34472×7659 system matrix, $\mathbf{a}$ is a 7659-element column vector of spline coefficients, and $\mathbf{p}$ is a 34472-element column vector of modeled projection values.

Using a dual-processor 2.5-GHz PowerPC G5 Macintosh with 8 GB of memory and MATLAB software, the penalized least-squares volumetric image reconstruction took about 9 cpu-min and involved seven iterations of steps 4 and 5 in the algorithm described in Section II (i.e., a 7659×7659 matrix was inverted eight times). Post-reconstruction smoothing was performed in transverse planes with a separable 3×3 filter that smoothed spline coefficients with a [1/4 1/2 1/4] kernel first along the x-axis and then along the y-axis. Rows 1 and 2 of Fig. 4 show transverse cross-sections through the 3-D image volume reconstructed without use of and with use of the negativity penalty, respectively. Use of the penalty dramatically reduced image noise for the higher-resolution basis and yielded good resolution throughout the body (row 2).

For the multiresolution spatial basis, the penalized least-squares volumetric image reconstruction took only about 0.8 cpu-min and involved four iterations of steps 4 and 5 in the algorithm described in Section II (i.e., a 2626×2626 matrix was inverted five times). Post-reconstruction smoothing in transverse planes was performed only on higher-resolution spline coefficients in the heart volume with a separable 3×3 filter that smoothed with a [1/4 1/2 1/4] kernel first along the x-axis and then along the y-axis. Rows 3 and 4 of Fig. 4 show transverse cross-sections through the 3-D image volume reconstructed without use of and with use of the negativity penalty, respectively. The negativity penalty had only a subtle

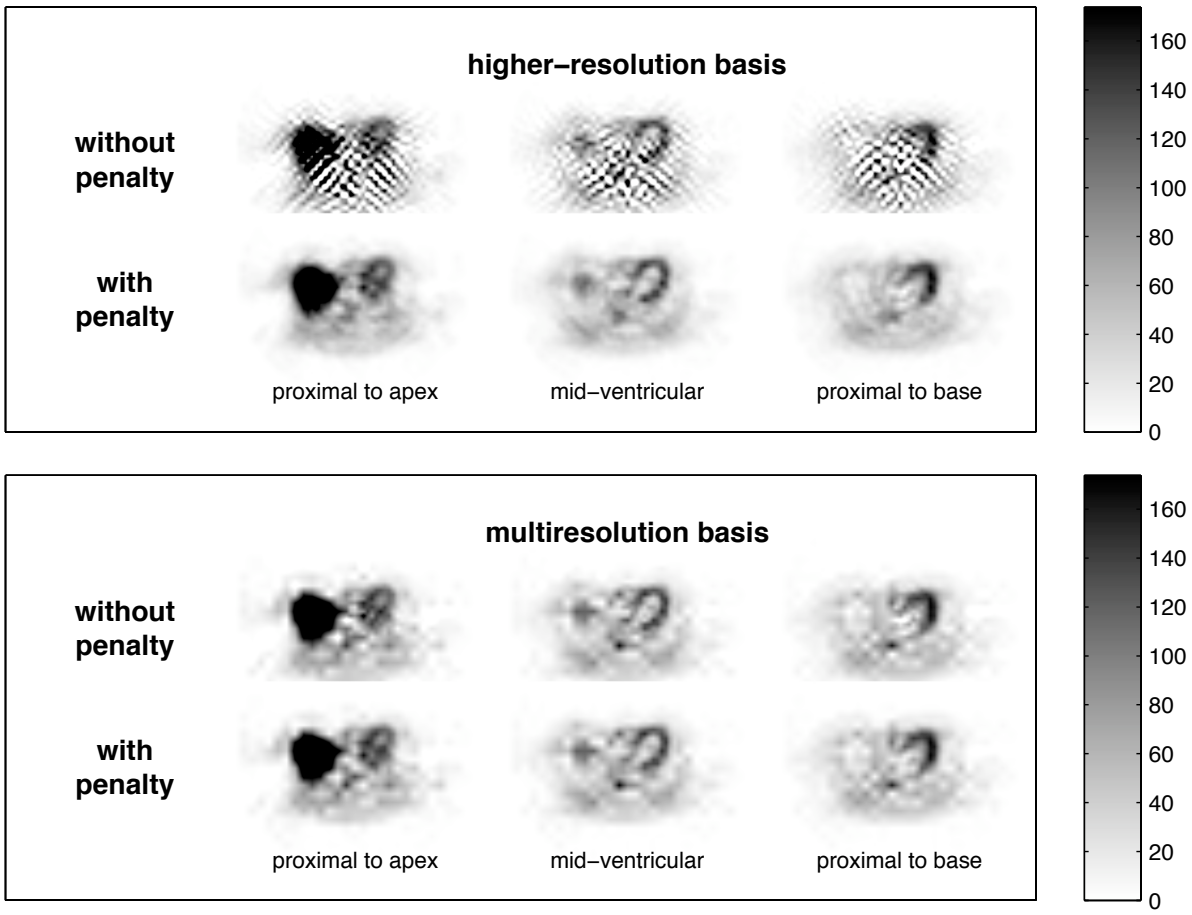

Fig. 4. Transverse cross-sections through the 3-D image volume modeled with higher-resolution splines (rows 1 and 2) and multiresolution splines (rows 3 and 4) and reconstructed without use of (rows 1 and 3) and with use of (rows 2 and 4) the negativity penalty. Use of the penalty dramatically reduces image noise for the higher-resolution splines and yields good resolution throughout the body (row 2). The negativity penalty has only a subtle effect for the multiresolution splines (row 4), as noise is already well-controlled by the lower-resolution splines used to model the volume outside the heart (row 3).

effect (row 4), as noise was already well-controlled by the lower-resolution splines used to model the volume outside the heart (row 3)

V. Conclusion

A negativity penalty was straightforwardly introduced into a fully 3-D least-squares SPECT image reconstruction algorithm. Use of the penalty dramatically reduced noise and yielded good spatial resolution for an image volume that was modeled with higher-resolution B-spline spatial basis functions and was reconstructed by direct matrix inversion via Cholesky decomposition.

Encouraged by these results, we are using multiresolution 4-D spatiotemporal B-splines and penalized weighted least-squares inversion to reconstruct dynamic SPECT data from rest/stress cardiac patient studies.

References

[1] B. W. Reutter, G. T. Gullberg, A. Sitek, R. Boutchko, E. H. Botvinick, and R. H. Huesman, "Modeling spatial smoothness in fully 3-D SPECT image reconstruction using multiresolution B-splines," in *2006 IEEE Nuclear Science Symposium and Medical Imaging Conference Record*, B. Phlips, Ed., 2006, pp. 1757–1761.

[2] W. H. Press, S. A. Teukolsky, W. T. Vetterling, and B. P. Flannery, *Numerical Recipes in C: The Art of Scientific Computing*, 2nd ed. Cambridge, England: Cambridge University Press, 1992.

[3] R. M. Lewitt, "Multidimensional digital image representations using generalized Kaiser-Bessel window functions," *J Opt Soc Am A*, vol. 7, no. 10, pp. 1834–1846, 1990.

[4] S. Horbelt, M. Liebling, and M. Unser, "Discretization of the Radon transform and of its inverse by spline convolutions," *IEEE Trans Med Imag*, vol. 21, no. 4, pp. 363–376, 2002.

[5] A. Yendiki and J. A. Fessler, "A comparison of rotation- and blob-based system models for 3D SPECT with depth-dependent point response," *Phys Med Biol*, vol. 49, no. 11, pp. 2157–2168, 2004.

[6] J. S. Maltz, "Optimal time-activity basis selection for exponential spectral analysis: Application to the solution of large dynamic emission tomographic reconstruction problems," *IEEE Trans Nucl Sci*, vol. 48, no. 3, pp. 1452–1464, 2001.

[7] R. H. Bartels, J. C. Beatty, and B. A. Barsky, *An Introduction to Splines for Use in Computer Graphics and Geometric Modeling*. Los Altos, CA: Morgan Kaufmann, 1987.

[8] M. Unser, "Splines: A perfect fit for signal and image processing," *IEEE Signal Processing Magazine*, vol. 16, no. 6, pp. 22–38, 1999.

[9] G. L. Zeng, G. T. Gullberg, B. M. W. Tsui, and J. A. Terry, "Three-dimensional iterative reconstruction algorithms with attenuation and geometric point response correction," *IEEE Trans Nucl Sci*, vol. 38, no. 2, pp. 693–702, 1991.